A Control Theoretical Adaptive Human Pilot Model: Theory and Experimental Validation

Seyed Shahabaldin Tohidi and Yildiray Yildiz, *Senior Member, IEEE*

***Abstract*— This article proposes an adaptive human pilot model that is able to mimic the crossover model in the presence of uncertainties. The proposed structure is based on the model reference adaptive control, and the adaptive laws are obtained using the Lyapunov–Krasovskii stability criteria. The model can be employed for human-in-the-loop stability and performance analyses incorporating different types of controllers and plant types. For validation purposes, an experimental setup is employed to collect data and a statistical analysis is conducted to measure the predictive power of the pilot model.**

***Index Terms*— Adaptive control, control of time-delay systems, crossover model, human decision-making, pilot modeling, uncertain systems.**

I. Introduction

HUMANS' unique abilities, such as adaptive behavior in dynamic environments, and social interaction and moral judgment capabilities, make them essential elements of many control loops. On the other hand, compared to humans, automation provides higher computational performance and multitasking capabilities without any fatigue, stress, or boredom [1], [2]. Although they have their own individual strengths, humans and automation also demonstrate several weaknesses. Humans may have anxiety and fear and may become unconscious during an operation. Furthermore, in the tasks that require increased attention and focus, humans tend to provide high-gain control inputs that can cause undesired oscillations. One example of this phenomenon, for example, is the occurrence of pilot-induced oscillations (PIOs), where undesired and sustained oscillations are observed due to an abnormal coupling between the aircraft and the pilot [3]–[6]. Similarly, automation may fail due to uncertainty, fault, or cyberattack [7]. Thus, it is more preferable to design systems where humans and automation work in harmony, complementing each other, resulting in a structure that benefits from the advantages of both.

To achieve a reliable human-automation harmony, a mathematically rigorous human operator model is paramount. A human operator model helps develop safe control systems and provides a better prediction of human actions and limitations [8]–[11]. Quasi-linear model [12] is one of the first human operator models, which consists of a describing function and a remnant signal accounting for nonlinear behavior. An overview of this model is provided in [13]. In some applications, where the linear behavior may be dominant, the nonlinear part of this model can be ignored, and the resulting lead-lag-type compensator is used in the closed-loop stability analysis [14]. The crossover model, proposed in [15], is another important human operator model in the aerospace domain. It is motivated from the empirical observations that human pilots adapt their responses in such a way that the overall system dynamics resembles that of a well-designed feedback system [16]. A generalized crossover model, which mimics human behavior when controlling a fractional-order plant, is proposed in [17]. In [18], a crossover model is employed to provide information about the human intent for the controller. In [19], the dynamics of the operator is represented as a spring–damper–mass system.

Control theoretical operator models employing optimal and adaptive control theories are also proposed by several authors. Optimal human models are based on the idea that a well-trained human operator behaves in an optimal manner [20]–[24]. On the other hand, adaptive models, such as the ones proposed in [25] and [26], aim to replicate the adaptation capability of humans in uncertain and dynamics environments. In [25] and [26], adaptation rules are proposed based on expert knowledge. The adaptive model proposed in [25] is applied to change the parameters of the pilot model based on force feedback from a smart inceptor [27]. A survey on various pilot models can be found in [28] and [29].

Several approaches are also developed for human model parameter identification. In [30], a two-step method using wavelets and a windowed maximum likelihood estimation are exploited for the estimation of time-varying pilot model parameters. In [31], a linear parameter-varying model identification framework is incorporated to estimate time-varying human state-space representation matrices. Subsystem identification is used in [32] to model human control strategies. In [33], a human operator model for preview tracking tasks is derived from the measurement data.

Manuscript received 31 May 2021; revised 20 December 2021; accepted 2 March 2022. Date of publication 19 April 2022; date of current version 21 October 2022. This work was supported in part by the Scientific and Technological Research Council of Turkey under Grant 118E202 and in part by the Turkish Academy of Sciences through the Young Scientist Award Program. Recommended by Associate Editor M. Oishi. *(Corresponding author: Seyed Shahabaldin Tohidi.)*

This work involved human subjects or animals in its research. Approval of all ethical and experimental procedures and protocols was granted by the Bilkent University Ethics Committee.

Seyed Shahabaldin Tohidi is with the Applied Mathematics and Computer Science Department, Technical University of Denmark, 2800 Kongens Lyngby, Denmark (e-mail: sshto@dtu.dk).

Yildiray Yildiz is with the Faculty of Mechanical Engineering, Bilkent University, 06800 Ankara, Turkey (e-mail: yyildiz@bilkent.edu.tr).

Color versions of one or more figures in this article are available at https://doi.org/10.1109/TCST.2022.3164237.

Digital Object Identifier 10.1109/TCST.2022.3164237

In this article, we build upon the earlier successful pilot models and propose an adaptive human pilot model that modifies its behavior based on plant uncertainties. This model distinguishes itself from earlier adaptive models by having mathematically derived laws to achieve a crossover-model-like behavior, instead of employing expert knowledge. This allows a rigorous stability proof, using the Lyapunov–Krasovskii stability criteria, of the overall closed-loop system. Therefore, unlike earlier adaptive approaches, the design has formal guarantees to follow the crossover model in the presence of system uncertainty. Although expert knowledge can also be incorporated in the proposed design, it does not rely on this information to function. It is noted that in this article, we do not claim that the model we propose explains how the decisions are made by pilots. Rather, we propose an operator model that can make the overall system mimic the behavior of the crossover model. To validate the model, a setup, including a joystick and a monitor, is used. The participant data collected through this experimental setup are subjected to visual and statistical analyses to evaluate the accuracy of the proposed model. Initial research results of this study were presented in [34], where the details of the mathematical proof and human experimental validation studies were missing.

This article is organized as follows. In Section II, the problem statement is given. Obtaining reference model parameters, which determine the properties of the crossover model, is discussed in Section III. Section IV presents the human control strategy together with a stability analysis. Experimental setup, results, and a statistical analysis are provided in Section V. Finally, a summary is given in Section VI.

II. Problem Statement

According to McRuer's crossover model [35], human pilots in the control loop behave in a way that results in an open-loop transfer function

$$Y_{\text{OL}}(s) = Y_h(s)Y_p(s) = \frac{\omega_c e^{-\tau s}}{s} \tag{1}$$

near the crossover frequency, ω_c, where Y_h is the transfer function of the human pilot and Y_p is the transfer function of the plant. τ is the effective time delay, including transport delays and high-frequency neuromuscular lags. The input and the output of the closed-loop transfer function, whose near-crossover-frequency open-loop behavior is given in (1), are the desired (reference) and achieved trajectories.

Consider the following plant dynamics:

$$\begin{aligned} \dot{x}_p(t) &= A_p x_p(t) + B_p u_p(t) \\ y_p(t) &= C_p x_p(t) \end{aligned} \tag{2}$$

where $x_p \in \mathbb{R}^{n_p}$ is the plant state vector, $u_p \in \mathbb{R}$ is the input vector, $A_p \in \mathbb{R}^{n_p \times n_p}$ is an unknown state matrix, $B_p \in \mathbb{R}^{n_p}$ is an unknown input matrix, and $C_p \in \mathbb{R}^{1 \times n_p}$ is the known output matrix.

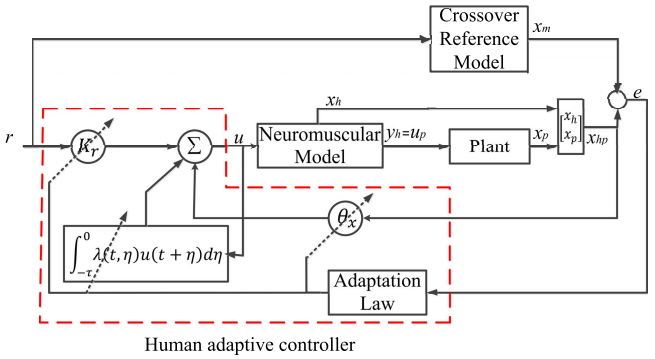

Fig. 1. Block diagram of the human adaptive behavior and decision-making in a closed-loop system.

The human neuromuscular model [36], [37] is represented in the state-space form as

$$\begin{aligned} \dot{x}_h(t) &= A_h x_h(t) + B_h u(t-\tau) \\ y_h(t) &= C_h x_h(t) + D_h u(t-\tau) \end{aligned} \tag{3}$$

where $x_h \in \mathbb{R}^{n_h}$ is the neuromuscular state vector, $A_h \in \mathbb{R}^{n_h \times n_h}$ is the state matrix, $B_h \in \mathbb{R}^{n_h}$ is the input matrix, $C_h \in \mathbb{R}^{1 \times n_h}$ is the output matrix, and $D_h \in \mathbb{R}$ is the control output matrix. $u \in \mathbb{R}$ is the neuromuscular input vector, which represents the control decisions taken by the human and fed to the neuromuscular system, $y_h \in \mathbb{R}$ is the output vector, and $\tau \in \mathbb{R}^+$ is a known, constant delay. The neuromuscular model parameters are assumed to be known and the output of the model, y_h, is used as the plant input u_p in (2), that is, $y_h = u_p$ (see Fig. 1).

By aggregating the human pilot and plant states, we obtain the combined open-loop human neuromuscular and plant dynamics as

$$\underbrace{\begin{bmatrix} \dot{x}_h(t) \\ \dot{x}_p(t) \end{bmatrix}}_{\dot{x}_{hp}(t)} = \underbrace{\begin{bmatrix} A_h & 0_{n_h \times n_p} \\ B_p C_h & A_p \end{bmatrix}}_{A_{hp}} \underbrace{\begin{bmatrix} x_h(t) \\ x_p(t) \end{bmatrix}}_{x_{hp(t)}} + \underbrace{\begin{bmatrix} B_h \\ B_p D_h \end{bmatrix}}_{B_{hp}} u(t-\tau) \tag{4}$$

which can be written in the following compact form:

$$\begin{aligned} \dot{x}_{hp}(t) &= A_{hp} x_{hp}(t) + B_{hp} u(t-\tau) \\ y_p(t) &= C_{hp} x_{hp}(t) \end{aligned} \tag{5}$$

where $x_{hp} = [x_h^T \; x_p^T]^T \in \mathbb{R}^{(n_p+n_h)}$, $A_{hp} \in \mathbb{R}^{(n_p+n_h)\times(n_p+n_h)}$, $B_{hp} \in \mathbb{R}^{(n_p+n_h)}$, and $C_{hp} = [0_{1\times n_h} \; C_p] \in \mathbb{R}^{1\times(n_p+n_h)}$.

Assumption 1: The pair (A_{hp}, B_{hp}) is controllable.

The goal is to obtain the input $u(t)$ in (3), which is the output of the human decision-making process, such that the closed-loop system consisting of the adaptive human pilot model and the plant follow the output of a unity feedback reference model with an open-loop crossover model transfer function. We call this reference model as "crossover reference model" (see Fig. 1). It is noted that once $u(t)$ is created, it is used as the input to the neuromuscular model, which creates the pilot motion. To summarize, assuming that the neuromuscular model, the parameters to determine the crossover model reference model, and the structure of the

TABLE I
DEPENDENCY OF CROSSOVER FREQUENCY TO THE HIGHEST INPUT FREQUENCY (ω_i)

Plant transfer function	Crossover frequency of the open loop transfer function (rad/s)
K	$\omega_c = 0.067\omega_i^2 + 0.099\omega_i + 4.8$
K/s	$\omega_c = 0.14\omega_i + 4.3$
K/s^2	$\omega_c = -0.0031\omega_i^4 - 0.072\omega_i^3 + 0.29\omega_i^2 - 0.13\omega_i + 3$

plant with parametric uncertainties are available, we aim to find the evolution of the output of the human decision-making process, which is represented by the variable $u(t)$, such that the closed-loop model (including the decision-making process, human neuromuscular model, and plant model) matches the crossover reference model.

The closed-loop transfer function of the reference model is therefore calculated as

$$G_{\text{cl}}(s) = \frac{\frac{\omega_c}{s}e^{-\tau s}}{1 + \frac{\omega_c}{s}e^{-\tau s}} = \frac{\omega_c e^{-\tau s}}{s + \omega_c e^{-\tau s}}. \tag{6}$$

An approximation of (6) can be given as

$$\hat{G}_{\text{cl}}(s) = \frac{b_m s^m + b_{m-1}s^{m-1} + \cdots + b_0}{s^n + a_{n-1}s^{n-1} + \cdots + a_0}e^{-\tau s} \tag{7}$$

where $n = n_h + n_p$ and $m \leq n$ are positive real constants, and a_i and b_j for $i = 0, \ldots, n-1$ and $j = 0, \ldots, m-1$, are real constants to be estimated. The reference model then can be obtained as the state-space representation of (7) as

$$\begin{aligned} \dot{x}_m(t) &= A_m x_m(t) + B_m r(t-\tau) \\ y_m(t) &= C_m x_m(t) \end{aligned} \tag{8}$$

where $x_m \in \mathbb{R}^{(n_h+n_p)}$ is the reference model state vector, $A_m \in \mathbb{R}^{(n_h+n_p)\times(n_h+n_p)}$ is the state matrix, $B_m \in \mathbb{R}^{(n_h+n_p)\times m_h}$ is the input matrix, $C_m \in \mathbb{R}^{1\times(n_h+n_p)}$ is the output matrix, and $r \in \mathbb{R}^{m_h}$ is the reference input. It is noted that C_m is selected to be equal to C_{hp}.

III. REFERENCE MODEL PARAMETERS

The crossover transfer function (1) contains the crossover frequency, ω_c, which is not known *a priori*. Experimental data, showing the reference input ($r(t)$) frequency bandwidth, ω_i, versus crossover frequency ω_c, is provided in [16] and [35], for plant transfer functions K, K/s, and K/s^2. We fit polynomials to these experimental results to obtain the crossover frequency of the open-loop transfer function given a reference input frequency bandwidth. These polynomials are given in Table I. It is noted that when the reference input has multiple frequency components, the highest frequency is used to calculate the crossover frequency.

Remark 2: In this work, we use the polynomial relationships provided in Table I for zero-, first-, and second-order plant dynamics with nonzero poles and zeros. Further experimental work can be conducted to obtain a more precise relationship between the crossover and reference input frequencies, but this is currently out of the scope of this work.

IV. HUMAN PILOT CONTROL DECISION COMMAND

The adaptive human pilot control decision command, $u(t)$, is determined as

$$u(t) = K_r K_x \hat{x}_{hp}(t+\tau) + K_r r(t) \tag{9}$$

where $K_x \in \mathbb{R}^{1\times(n_h+n_p)}$, $K_r \in \mathbb{R}^{m_h\times m_h}$, and $\hat{x}_{hp} \in \mathbb{R}^{(n_p+n_h)}$ is the predicted value for x_{hp}. Using (5) and (9), the closed-loop dynamics can be obtained as

$$\dot{x}_{hp}(t) = (A_{hp} + B_{hp}K_r K_x)\hat{x}_{hp}(t) + B_{hp}K_r r(t-\tau). \tag{10}$$

Assumption 3: There exist ideal parameters K_r^* and K_x^* satisfying the following matching conditions:

$$\begin{aligned} A_{hp} + B_{hp}K_r^* K_x^* &= A_m \\ B_{hp}K_r^* &= B_m. \end{aligned} \tag{11}$$

Equation (9) describes a noncausal decision command, which requires future values of the states. This problem can be eliminated by solving the differential equation (5) as a τ-seconds ahead predictor as

$$\hat{x}_{hp}(t+\tau) = e^{A_{hp}\tau}x_{hp}(t) + \int_{-\tau}^{0} e^{-A_{hp}\eta}B_{hp}u(t+\eta)d\eta. \tag{12}$$

By substituting (12) into (9), the human pilot control decision input can be written as

$$\begin{aligned} u(t) = {} & K_r K_x e^{A_{hp}\tau}x_{hp}(t) \\ & + K_r K_x \int_{-\tau}^{0} e^{-A_{hp}\eta}B_{hp}u(t+\eta)d\eta + K_r r(t). \end{aligned} \tag{13}$$

By defining $\theta_x(t)$ and $\lambda(t,\eta)$ as

$$\begin{aligned} \theta_x(t) &= K_r(t)K_x(t)e^{A_{hp}\tau} \\ \lambda(t,\eta) &= K_r(t)K_x(t)e^{-A_{hp}\eta}B_{hp} \end{aligned} \tag{14}$$

(13) can be rewritten as (see Fig. 1)

$$u(t) = \theta_x(t)x_{hp}(t) + \int_{-\tau}^{0}\lambda(t,\eta)u(t+\eta)d\eta + K_r(t)r(t). \tag{15}$$

Since A_{hp} and B_{hp} are unknown, θ_x, λ, and K_r need to be estimated. It is noted that (11) presents the equation that define the ideal value of K_r, which is denoted as K_r^*. Comparing (13) and (15), the ideal values of θ_x and λ can be obtained as

$$\begin{aligned} \theta_x^* &= K_r^* K_x^* e^{A_{hp}\tau} \\ \lambda^*(\eta) &= K_r^* K_x^* e^{-A_{hp}\eta}B_{hp}. \end{aligned} \tag{16}$$

The closed-loop dynamics can be obtained using (5) and (15) as

$$\begin{aligned} \dot{x}_{hp}(t) = {} & A_{hp}x_{hp}(t) + B_{hp}\theta_x(t-\tau)x_{hp}(t-\tau) \\ & + \int_{-\tau}^{0} B_{hp}\lambda(t-\tau,\eta)u(t+\eta-\tau)d\eta \\ & + B_{hp}K_r r(t-\tau). \end{aligned} \tag{17}$$

Defining the deviations of the adaptive parameters from their ideal values as $\tilde{\theta}_x = \theta_x - \theta_x^*$ and $\tilde{\lambda} = \lambda - \lambda^*$, adding and

subtracting $A_m x_{hp}(t)$ to (17), and using (11), we obtain that

$$\begin{aligned}\dot{x}_{hp}(t) = {} & A_m x_{hp}(t) - B_{hp}K_r^* K_x^* x_{hp}(t) \\ & + B_{hp}K_r(t-\tau)K_x(t-\tau) \\ & \times \left(e^{A_{hp}\tau}x_{hp}(t-\tau) + \int_{-\tau}^{0} e^{-A_{hp}\eta}B_{hp}u(t+\eta-\tau)d\eta\right) \\ & + B_{hp}K_r(t-\tau)r(t-\tau). \end{aligned} \tag{18}$$

Using (12), (18) is rewritten as

$$\begin{aligned}\dot{x}_{hp}(t) = {} & A_m x_{hp}(t) - B_{hp}K_r^* K_x^* x_{hp}(t) \\ & + B_{hp}K_r(t-\tau)K_x(t-\tau)x_{hp}(t) \\ & + B_{hp}K_r(t-\tau)r(t-\tau). \end{aligned} \tag{19}$$

Defining the tracking error as $e(t) = x_{hp} - x_m$, subtracting (8) from (19), using (11), and following a similar procedure given in [38], it is obtained that:

$$\begin{aligned}\dot{e}(t) = {} & \dot{x}_{hp} - \dot{x}_m \\ = {} & A_m e(t) - B_{hp}K_r^* K_x^* x_{hp}(t) \\ & + B_{hp}K_r(t-\tau)K_x(t-\tau)x_{hp}(t) \\ & + B_{hp}\big(K_r(t-\tau) - K_r^*\big)r(t-\tau) \\ = {} & A_m e(t) + \big(-B_{hp}K_r^* K_x^* + B_{hp}\big(K_r^* - K_r^* + K_r(t-\tau)\big) \\ & \times K_x(t-\tau)\big)x_{hp}(t) \\ & + B_{hp}\big(K_r(t-\tau) - K_r^*\big)r(t-\tau) \\ = {} & A_m e(t) + B_m\big(K_x(t-\tau) - K_x^*\big)x_{hp}(t) \\ & + B_m\big(K_r^{*-1}K_r(t-\tau) - 1\big)K_x(t-\tau)x_{hp}(t) \\ & + B_m\big(K_r^{*-1}K_r(t-\tau) - 1\big)r(t-\tau) \\ = {} & A_m e(t) + B_m(\tilde{K}_x(t-\tau)x_{hp}(t) \\ & + B_m\big(K_r^{*-1} - K_r^{-1}(t-\tau)\big)K_r(t-\tau)K_x(t-\tau)x_{hp}(t) \\ & + B_m\big(K_r^{*-1} - K_r^{-1}(t-\tau)\big)K_r(t-\tau)r(t-\tau). \end{aligned} \tag{20}$$

Using (12) and defining $\Phi = K_r^{*-1} - K_r^{-1}$, we can rewrite (20) as

$$\begin{aligned}\dot{e}(t) = {} & A_m e(t) + B_m K_r^{*-1}\big(K_r^* K_x(t-\tau) - K_r^* K_x^*\big) \\ & \times \left(e^{A_{hp}\tau}x_{hp}(t-\tau) + \int_{-\tau}^{0} e^{-A_{hp}\eta}B_{hp}u(t+\eta-\tau)d\eta\right) \\ & + B_m\Phi(t-\tau)\Bigg(K_r(t-\tau)K_x(t-\tau)\Bigg(e^{A_{hp}\tau}x_{hp}(t-\tau) \\ & + \int_{-\tau}^{0} e^{-A_{hp}\eta}B_{hp}u(t+\eta-\tau)d\eta\Bigg) \\ & + K_r(t-\tau)r(t-\tau)\Bigg). \end{aligned} \tag{21}$$

Using (16) and (21), we obtain that

$$\begin{aligned}\dot{e}(t) = {} & A_m e(t) + B_m K_x(t-\tau) \\ & \times\left(e^{A_{hp}\tau}x_{hp}(t-\tau) + \int_{-\tau}^{0} e^{-A_{hp}\eta}B_{hp}u(t+\eta-\tau)d\eta\right) \\ & - B_m K_r^{*-1}\left(\theta_x^* x_{hp}(t-\tau) + \int_{-\tau}^{0}\lambda^*(\eta)u(t+\eta-\tau)d\eta\right) \\ & + B_m\Phi(t-\tau)u(t-\tau). \end{aligned} \tag{22}$$

Using (14), (22) can be rewritten as

$$\begin{aligned}\dot{e}(t) = {} & A_m e(t) + B_m \\ & \times\Bigg(\big(K_r^{-1}(t-\tau)\theta_x(t-\tau) - K_r^{*-1}\theta_x^*\big) \\ & \times x_{hp}(t-\tau) + \int_{-\tau}^{0}\big(K_r^{-1}(t-\tau)\lambda(t-\tau,\eta) \\ & - K_r^{*-1}\lambda^*(\eta)\big)u(t+\eta-\tau)d\eta\Bigg) \\ & + B_m\Phi(t-\tau)u(t-\tau). \end{aligned} \tag{23}$$

Defining $\theta_1 = K_r^{-1}\theta_x$ and $\lambda_1 = K_r^{-1}\lambda$ and using their deviations from their ideal values, $\tilde{\theta}_1 = \theta_1 - \theta_1^*$ and $\tilde{\lambda}_1 = \lambda_1 - \lambda_1^*$, where $\theta_1^* = K_r^{*-1}\theta_x^*$ and $\lambda_1^* = K_r^{*-1}\lambda^*$, (23) can be rewritten as

$$\begin{aligned}\dot{e}(t) = {} & A_m e(t) + B_m\tilde{\theta}_1(t-\tau)x_{hp}(t-\tau) \\ & + B_m\int_{-\tau}^{0}\tilde{\lambda}_1(t-\tau,\eta)u(t+\eta-\tau)d\eta \\ & + B_m\Phi(t-\tau)u(t-\tau). \end{aligned} \tag{24}$$

The following lemma will be necessary to prove the main theorem of this article.

Lemma 4: Suppose that the continuous function $u(t)$ is given as

$$u(t) = f(t) + \int_{-\tau}^{0}\lambda(t,\eta)u(t+\eta)d\eta \tag{25}$$

where $u, f : [t_0 - \tau, \infty] \to R$ and $\lambda : [t_0, \infty) \times [-\tau, 0] \to R$. Then

$$|u(t)| \le 2(\bar{f} + c_0 c_1)e^{c_0^2(t-t')} \quad \forall t_j' \ge t_i' \tag{26}$$

if constants t_i', $\bar{f}$, $c_0, c_1 \in R^+$ exist such that $|f(t)| \le \bar{f}$

$$\int_{-\tau}^{0}\lambda^2(t,\eta)d\eta \le c_0^2, \quad \text{for } t \in \left[t_i', t_j'\right) \tag{27}$$

and

$$\int_{-\tau}^{0}u^2(t+\eta)d\eta \le c_1^2 \quad \forall t \le t_i'. \tag{28}$$

Proof: The proof of Lemma 4 can be found in [39]. □

Theorem 5: Given the initial conditions $\tilde{\theta}_1(\xi)$, $\tilde{\lambda}_1(\xi,\eta)$, $\Phi(\xi)$ and $x_{hp}(\xi)$ for $\xi \in [-\tau, 0]$, and $u(\zeta)$ for $\zeta \in [-2\tau, 0]$, there exists τ^* such that for all $\tau \in [0, \tau^*]$, the controller (15) with the adaptive laws

$$\dot{\theta}_1^T(t) = -x_{hp}(t-\tau)e(t)^T P B_m \tag{29}$$

$$\dot{\Phi}^T(t) = -u(t-\tau)e(t)^T P B_m \tag{30}$$

$$\dot{\lambda}_1^T(t,\eta) = -u(t+\eta-\tau)e(t)^T P B_m \tag{31}$$

where P is the symmetric positive definite matrix satisfying the Lyapunov equation $A_m^T P + P A_m = -Q$ for a symmetric positive definite matrix Q, which can be employed to obtain controller parameters using $\dot{K}_r = \text{Proj}(K_r\dot{\Phi}K_r)$, $\theta_x(t) = K_r(t)\theta_1(t)$, and $\lambda(t) = K_r(t)\lambda_1(t)$ and make the pilot neuromuscular and plant aggregate system (5) follow the crossover reference model (8) asymptotically, i.e., $lim_{t\to\infty}x_{hp}(t) = x_m(t)$, while keeping all the signals bounded.

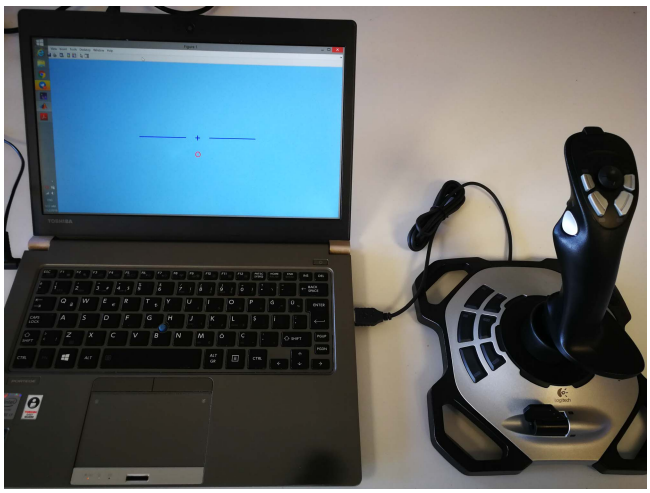

Fig. 2. Experimental setup.

Proof: The proof of this theorem is provided in the Appendix. □

The implementation of the proposed model requires the determination of: 1) the reference/crossover model and 2) the adaptive decision maker (see Fig. 1). A step-by-step procedure to design these two components is provided in the following.

Reference Model:

Step 1: Determine the maximum input frequency (frequency bandwidth) and the type of the plant transfer function.

Step 2: Using Table I, calculate the crossover frequency.

Step 3: Substitute the calculated crossover frequency (ω_c) and an estimate of human reaction delay (τ) in (6), calculate (7), and construct (8).

Adaptive Decision Maker:

Step 4: Use (15) as adaptive decision command.

Step 5: Use (29)–(31) as adaptive laws along with $\dot{K}_r = \text{Proj}(K_r \dot{\Phi} K_r)$, $\theta_x(t) = K_r(t)\theta_1(t)$, and $\lambda(t) = K_r(t)\lambda_1(t)$, where the details of the Proj operator can be found in [40] and [41].

V. Experimental Results

A. Experimental Environment

In order to test the proposed adaptive human model against data, an experimental setup consisting of a Logitech Extreme 3D Pro joystick and a Toshiba Portege-Z30-B laptop with Intel Core i7 CPU is used (see Fig. 2).

The tracking task is performed by an operator monitoring the pursuit display, which provides information about the error between the target to be followed and follower, which is the output of the plant (see Fig. 3). The operator provides the input u_p (see Fig. 1) through the joystick, which is fed to the plant using MATLAB/Simulink (R2018b). In return, the response of the plant is calculated and shown on the laptop screen in real time.

The reference signal $r(t)$ is generated as a sum of the sinusoids with frequencies of 0.1, 0.3, 0.5, 0.7, 1, 1.3, and 1.5 rad/s with the same amplitude of 0.2 and without phase shift.

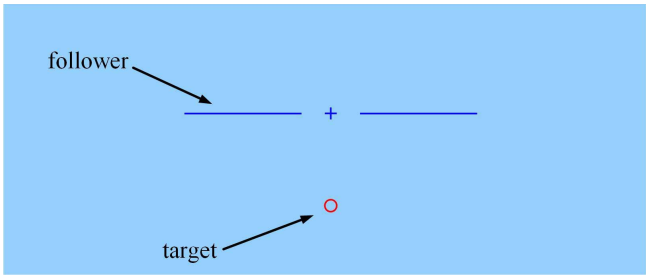

Fig. 3. Pursuit display.

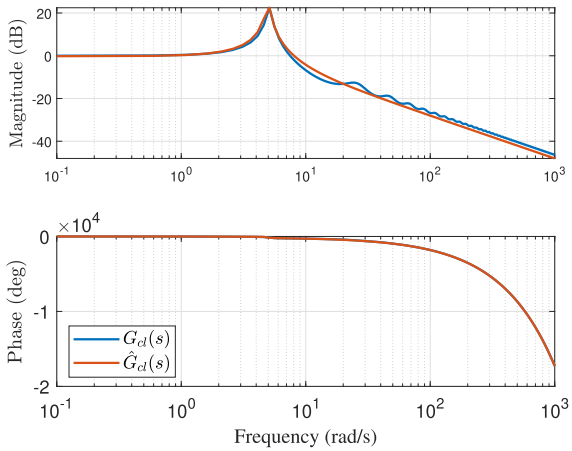

Fig. 4. Bode plot of the reference model and its approximation.

Three classes of plant models, having zero-, first-, and second-order transfer functions, are used in the experiments. In this section, we first give a detailed analysis of the first-order plant case and then provide a summary of the results of the other cases in tables. The nominal first-order plant used in the experiments is $Y_p(s) = (4/(s+1))$, which is similar to the one used in [25]. The uncertainty is introduced to the plant model by modifying the gain and the pole location by 50% to obtain $Y_p(s) = (6/(s+0.5))$.

To form the reference model (8), two parameters, namely, the crossover frequency and the time delay, need to be determined. The highest frequency component of the reference signal is $\omega_i = 1.5$ rad/s. Employing Table I for the first-order plant Y_p, the crossover frequency is calculated as $\omega_c = 4.5$ rad/s. The delay is determined by using the mean value of the operators' delay, which is $\tau = 0.3$ s. Therefore, the closed-loop transfer function of the reference model is calculated as

$$G_{\text{cl}}(s) = \frac{\frac{4.5}{s}e^{-0.3s}}{1+\frac{4.5}{s}e^{-0.3\ s}} = \frac{4.5\ e^{-0.3\ s}}{s+4.5\ e^{-0.3\ s}}. \tag{32}$$

Similar to (7), an approximate transfer function is obtained as

$$\hat{G}_{\text{cl}}(s) = \frac{3.881s+24.24}{s^2+0.6834s+24.72}e^{-0.3s}. \tag{33}$$

Fig. 4 shows a comparison between (32) and (33) and demonstrates that the approximation works well for almost all frequencies.

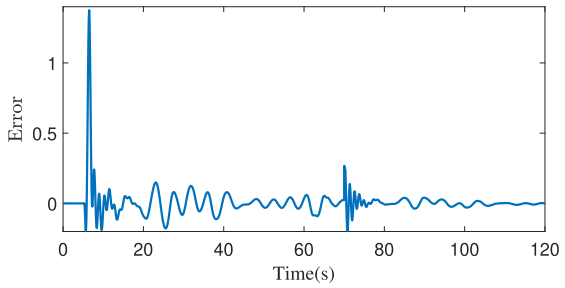

Fig. 5. Time evolution of the error between the output of the plant controlled by the adaptive model and the reference model output.

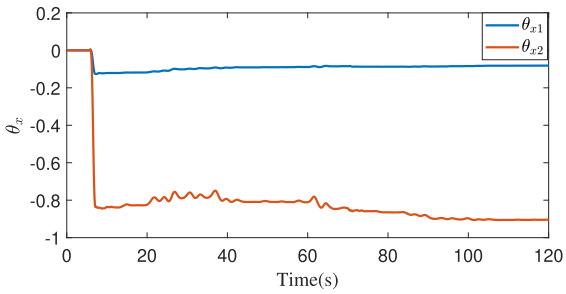

Fig. 6. Evolution of human adaptive parameters θ_{x1} and θ_{x2}.

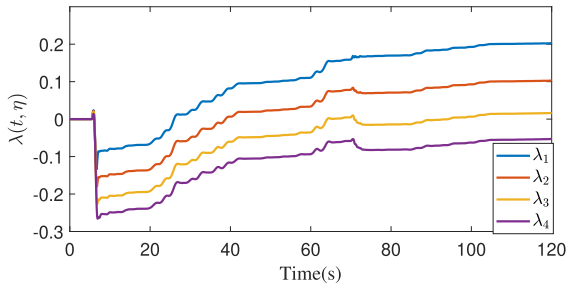

Fig. 7. Evolution of human adaptive parameters λ_i, $i = 1, 2, 3$, and 4.

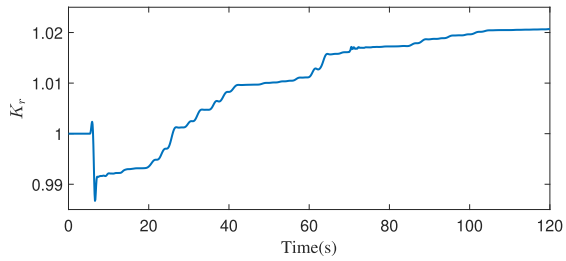

Fig. 8. Evolution of human adaptive parameter K_r.

The neuromuscular dynamics is taken as $Y_h(s) = ((s+3)/(s+2))e^{-0.3s}$, where the time delay $\tau = 0.3$ is the effective time delay, including human decision-making delay and neuromuscular lags.

Remark 6: In this article, we assume that the neuromuscular dynamics are given. The procedure for finding the neuromuscular model can be found in [36] and [37].

Remark 7: In [26], where decoupled multiaxis tracking tasks are considered, a factor is introduced to represent the fact that the pilots are less aggressive in multiaxis tasks, compared to single-axis ones. In this work, although we cover the single-axis tracking task, an extension to two-axis tracking would not need any new model development or an increase in complexity, except using the same equations stated in the step-by-step implementation guide in Section V, for the additional axis, with different gain and frequency parameters. A detailed analysis of single- and double-axis tracking tasks can be found in [42].

B. Behavior of the Adaptive Model

The error between the plant output and the reference model is shown in Fig. 5. The effect of uncertainty injection can be seen at $t = 70$ s. Figs. 6–8 show the adaptive human model parameters. To understand the amount of agreement between these results and the human experimental trials, visual and statistical analyses are provided in the following.

Remark 8: The model is developed based on adaptive control principles, and therefore, even when the plant model is not changing, the adaptive parameters may continue to vary based on the changes in the reference inputs. This parameter variance, however, is not a problem since the model's tracking capability, as well as the boundedness of the adaptive parameters, is guaranteed by the Lyapunov analysis. We also know that unless the inputs are persistently exciting, the adaptive parameters may not converge to their ideal values. Therefore, different trajectories may result in different model parameters. This is not an issue since these parameters are tuned automatically by the adaptive process.

Remark 9: Adaptation rates are important in terms of transient behavior, and therefore, their selection is important to obtain a successful model. There are some guidelines that can be used in the implementation, at least to start at a good initial condition for the tuning process [43], [44]. Consider a generic adaptive law $\dot{\theta} = -\Gamma e_1 \Omega$, where Γ is the adaptation rate matrix, e_1 is the tracking error, and Ω is the vector of corresponding system signals. Assuming that e_1 and elements of Ω are the same order of magnitude as the reference signal r, the adaptation rate for a parameter θ is chosen as $\Gamma = \theta^*/(3\tau_m \bar{r}^2)$, where θ^* is an estimate of the desired adaptive parameter, τ_m is the smallest time constant of the reference model, and $\bar{r}$ is the maximum possible amplitude of the reference signal.

C. Participants and Experimental Procedure

Eleven participants (six women and five men) from the graduate and undergraduate student pools of Bilkent University participated in the experiment. All of the participants read and signed the "informed consent to participate" document. This study is approved by the Bilkent University Ethics Committee for research with human participants. Before the experiments, to familiarize the participants with the experimental setup, and its environment, consisting of the display and the joystick, each participant was asked to follow a given reference via joystick inputs for the duration of 200 s. To prevent learning during these warm-up runs, the reference input, uncertainty injection times, and the uncertainty types were chosen differently from

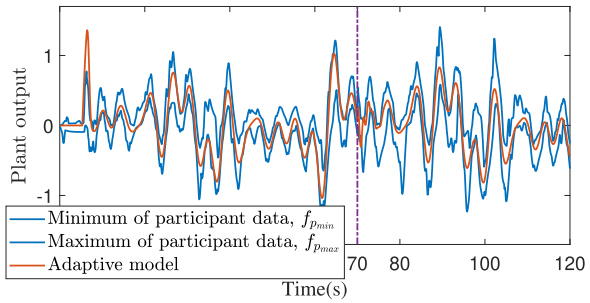

Fig. 9. Plant output, y_p, when adaptive human model is in the loop versus minimum and maximum values of plant output when participants are in the loop.

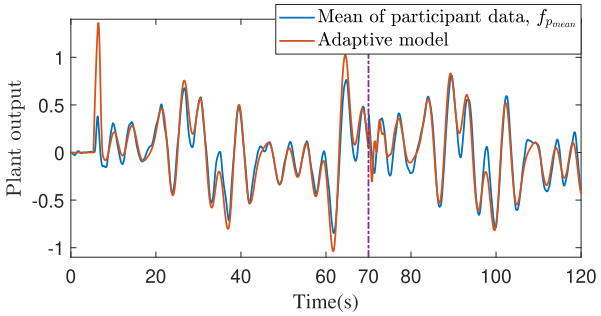

Fig. 10. Plant output, y_p, when adaptive human model is in the loop versus mean value of plant output when participants are in the loop.

the ones used in the real experimental runs. In particular, the reference signal for the warm-up runs consisted of the sum of the sinusoids with frequencies of 0.1, 0.5, 1, and 1.5 rad/s with the same amplitude of 0.2 and without phase shift. The plant dynamics at the beginning of the warm-up run was $(2/(s^2+3s+2))$. At $t = 45$ s, the dynamics changed to $(5/(s+2))$ in a step-like manner (suddenly). It is changed to $(3/(s+1))$ at around $t = 90$ s using a sigmoid function (gradually) and again changed to a zero-order dynamics at 150 s (suddenly).

D. Time- and Frequency-Domain Analyses of the Adaptive Model

Let $f_{p1}(t), f_{p2}(t), \ldots, f_{pk}(t)$ be the plant outputs when participants $p1, p2, \ldots, pk$ are in the loop, respectively. For each $f_{pi}(t)$, $t = T_1, T_2, \ldots, T_N$, where T_j, $j = 1, 2, \ldots, N$, represents a sampling instant, at each sampling instant T_j, the minimum, the maximum, and the mean values of the plant outputs when participants are in the loop can be obtained as

$$f_{p_{\min}}(T_j) = \min_{i=1,2,\ldots,k} f_{pi}(T_j), \quad j = 1, \ldots, N \tag{34}$$

$$f_{p_{\max}}(T_j) = \max_{i=1,2,\ldots,k} f_{pi}(T_j), \quad j = 1, \ldots, N \tag{35}$$

$$f_{p_{\text{mean}}}(T_j) = \frac{\sum_{i=1}^{k} f_{pi}(T_j)}{k}, \quad j = 1, \ldots, N \tag{36}$$

where $k = 11$ is the number of participants. Fig. 9 shows the evolutions of $f_{p_{\min}}$ and $f_{p_{\max}}$, together with $f_{\text{ad}}(t) \in \mathbb{R}^N$, which is the plant output when the adaptive human model is in the loop, where $t = T_1, T_2, \ldots, T_N$. It is seen that the plant output when adaptive human model is in the loop almost always stays

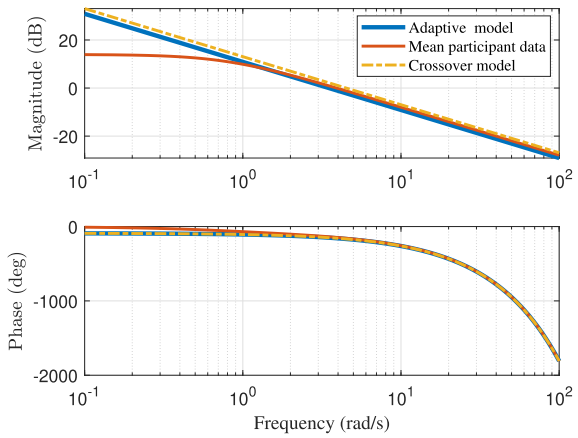

Fig. 11. Frequency responses of the crossover model, the adaptive model, and the mean human experimental data, before the uncertainty introduction.

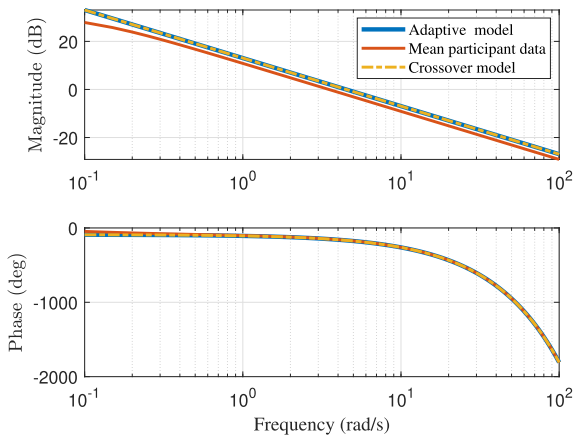

Fig. 12. Frequency responses of the crossover model, the adaptive model, and the mean human experimental data, after the uncertainty introduction.

between the maximum and the minimum values of the plant output when participants are in the loop. Furthermore, Fig. 10 shows that $f_{p_{\text{mean}}}$ and f_{ad} evolve reasonably close to each other.

The adaptive model and the mean participant data are also compared in the frequency domain both before and after the uncertainty introduction, in Figs. 11 and 12, respectively. As seen from the figures, both the adaptive model and participant data show similar properties with the crossover model. However, the model starts to deviate from the human data for lower frequencies. The transfer functions used to plot these Bode plots are obtained using the time-response data provided in Fig. 10. For the systems run by the adaptive model and the participants, we obtained the open-loop transfer functions $(3.5/s)e^{-0.3s}$ and $(4/(s+0.8))e^{-0.3s}$, respectively, before the uncertainty introduction, and $(4.5/s)e^{-0.3s}$ and $(3.5/(s+0.1))e^{-0.3s}$, after the uncertainty introduction. Fig. 13 shows the close match between the closed-loop time responses of the estimated transfer functions and the data used to obtain them.

E. Comparison Between the Adaptive and Fixed Human Models

In this section, to demonstrate the advantages of having an adaptive human model instead of a fixed one, we compare the behavior of these two models.

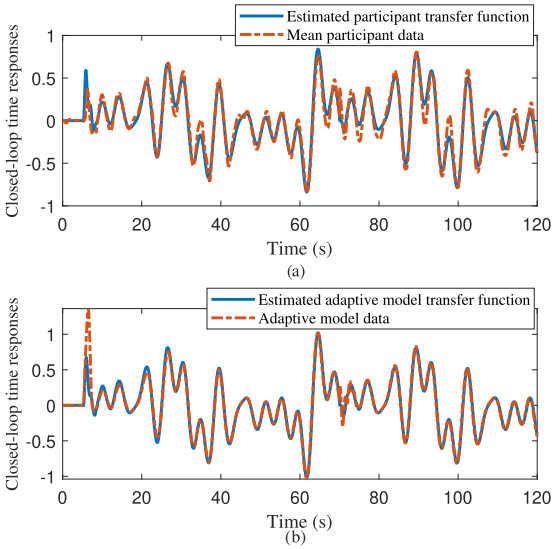

Fig. 13. Comparison between the closed-loop time response of estimated transfer functions and the data used to create them. (a) Participant transfer function and data. (b) Adaptive model transfer function and data.

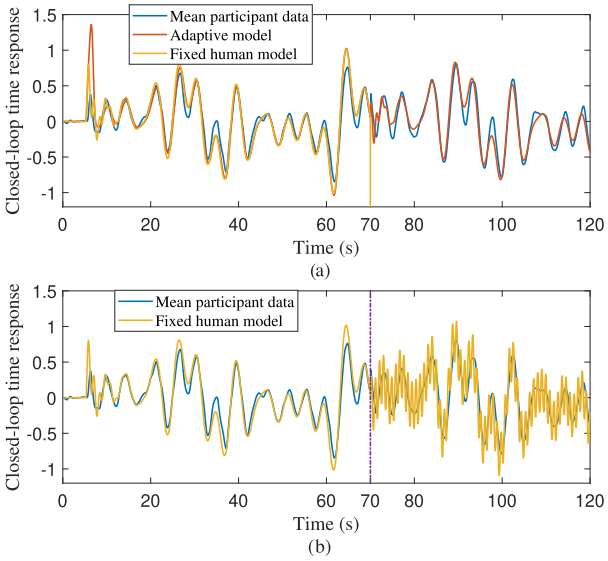

Fig. 14. Plant output, y_p, when the adaptive human model is in the loop versus fixed human model with (a) 0.3- and (b) 0.22-s time delay in the loop.

As the fixed human model, we use the transfer function $((1.125(s^2+3s+2))/(s^2+3s))e^{-0.3s}$, which makes the closed-loop transfer function equal to the crossover model given in (32).

Fig. 14(a) shows that before the occurrence of uncertainty at $t = 70$ s, both the fixed and the adaptive human models present a reasonable agreement with the experimental results. However, after the uncertainty introduction, the fixed model becomes unstable, while the adaptive model continues to show acceptable performance. The result demonstrates the danger of using a fixed model in the presence of time delays. Using the method proposed in [45], one can find that the system after the uncertainty introduction becomes unstable for delay values larger than 0.22 s. To provide a comparison in the stable region, we plot the response of the fixed model for a delay value of 0.22 s in Fig. 14(b). The plot shows that even though the response is stable, it fails to provide a reasonable prediction of the human pilot response after the uncertainty introduction.

F. Statistical Analysis of the Adaptive Model Using Confidence Intervals

The difference between the plant output when the ith participant is in the loop and when the adaptive human model is in the loop is defined as

$$d_i \equiv f_{\text{ad}} - f_{pi}, \quad i = 1, \ldots, k \tag{37}$$

where $d_i = [d_i(T_1), \ldots, d_i(T_N)]^T \in \mathbb{R}^N, i = 1, \ldots, k$, is called the ith difference. The mean and the standard deviation of the ith difference is obtained as

$$\bar{d}_i = \frac{\sum_{j=1}^{N} d_i(T_j)}{N}, \quad i = 1, \ldots, k \tag{38}$$

$$s_i = \sqrt{\frac{\sum_{j=1}^{N} (d_i(T_j) - \bar{d}_i)^2}{N-1}}, \quad i = 1, \ldots, k. \tag{39}$$

The normal-scores plot for $\bar{d}_i$ is shown in Fig. 15. The figure does not show any significant deviation from the normal

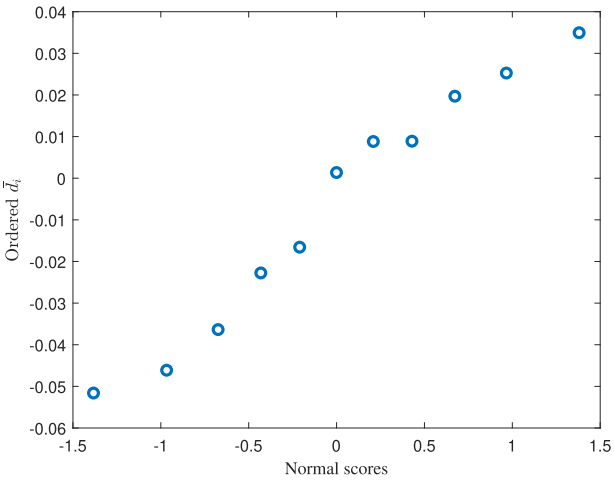

Fig. 15. Normal-scores plot.

distribution. This shows us that the data do not suggest that the population of mean errors, $\bar{d}_i$, deviates significantly from normal distribution. The sample mean and the sample standard deviation of $\bar{d}_i$'s can be obtained as

$$\bar{d} = \frac{\sum_{i=1}^{k} \bar{d}_i}{k} \tag{40}$$

$$s = \sqrt{\frac{\sum_{i=1}^{k} (\bar{d}_i - \bar{d})^2}{k-1}}. \tag{41}$$

Let μ_0 be the mean value of the population of mean errors, which is given as

$$\mu_0 \equiv \frac{\sum_{i=1}^{K} \bar{d}_i}{K} \tag{42}$$

where K is the population size. Since normal-scores plot, given in Fig. 15, did not provide any counter evidence, assuming that the distribution of the set of data $\{\bar{d}_1, \ldots, \bar{d}_K\}$ is normal with mean μ_0, μ_0 satisfies the following

probability [46]:

$$P\left[\bar{d} - t_{\alpha/2}\frac{s}{\sqrt{k}} < \mu_0 < \bar{d} + t_{\alpha/2}\frac{s}{\sqrt{k}}\right] = 1 - \alpha \qquad (43)$$

where $\bar{d}$ and s are obtained from (40) and (41), k is the number of participants, α is the significance level, and $t_{\alpha/2}$ is the upper $\alpha/2$ point of the t distribution with degree of freedom $k-1$, which can be obtained from the t-distribution table. Since the number of participants, $k = 11$, is less than 30, it is appropriate to use the t-distribution. Using $\alpha = 0.05$, obtaining $t_{\alpha/2}$ from the t-distribution table as 2.228, and calculating $\bar{d}$ as -0.0068 and s as 0.0379, it can be concluded using (43) that we are 95% confident that μ_0 is in the interval $(-0.0323, 0.0187)$. This shows that the mean μ_0 of the population's mean deviation from the adaptive human model is reasonably close to zero.

Similarly, the variance, σ_0^2, of the population's mean deviation from the adaptive human model satisfies the following probability [46]:

$$P\left[\frac{(k-1)s^2}{\chi^2_{\alpha/2}} < \sigma_0^2 < \frac{(k-1)s^2}{\chi^2_{1-\alpha/2}}\right] = 1 - \alpha \qquad (44)$$

where $\chi^2_{\alpha/2}$ is the upper $\alpha/2$ point of the χ^2 distribution with degree of freedom $k-1$ and can be obtained from the χ^2 distribution table. Calculating s from (41), using $\alpha = 0.05$, and obtaining $\chi^2_{\alpha/2}$ and $\chi^2_{1-\alpha/2}$ from the χ^2 table with ten degrees of freedom, it can be concluded using (44) that we are 95% confident that σ_0 is in the interval (0.0265, 0.0663). This shows that the standard deviation σ_0 of the population's mean deviation from the adaptive human model is reasonably small.

G. Statistical Analysis of the Adaptive Model Using Hypothesis Testing

In this analysis, we test whether the hypothesis "the mean value of the population mean errors, or the mean deviations from the adaptive model," is zero. In other words, our null hypothesis, H_0, is given as

$$H_0 : \mu_0 = 0 \qquad (45)$$

where μ_0 is defined in (42). The alternative hypothesis, H_1, is given as $H_1 : \mu \neq 0$. Similar to the confidence interval analysis, assuming that μ_0 is the mean of a normally distributed set of data $\{\bar{d}_1, \ldots, \bar{d}_K\}$, where K is the population size, the hypothesis H_0 is rejected if

$$\left|\frac{(\bar{d} - \mu_0)\sqrt{k}}{s}\right| \geq t_{\alpha/2} \qquad (46)$$

where $\bar{d}$ and s are obtained from (40) and (41), k is the number of participants, and $t_{\alpha/2}$ is the upper $\alpha/2$ point of the t distribution with degree of freedom $k-1$ [46]. Using the significance level $\alpha = 0.05$ and degree of freedom $k-1 = 10$, obtaining $t_{0.025} = 2.228$ from the t-distribution table, calculating $\bar{d} = -0.0068$ and $s = 0.038$ using (40) and (41), respectively, and substituting $\mu_0 = 0$ and $k = 11$, the left-hand side of (46) can be calculated as 0.5935, which is less than $t_{\alpha/2}$.

TABLE II
SUDDEN UNCERTAINTY

	0 order	1st order	2nd order
TF before 70 s	4	$\frac{4}{s+1}$	$\frac{4}{(s+1)(s+5)}$
TF after 70 s	6	$\frac{6}{s+0.5}$	$\frac{6}{(s+0.5)(s+2.5)}$
$\bar{d}$	0.0085	-0.0068	0.0011
s	0.0339	0.0379	0.0252
Mean conf. int.	$(-0.014, 0.03)$	$(-0.032, 0.02)$	$(-0.016, 0.018)$
St.d. conf. int.	$(0.024, 0.06)$	$(0.026, 0.066)$	$(0.018, 0.044)$
Hypothesis test	H_0 is retained	H_0 is retained	H_0 is retained

TABLE III
GRADUAL UNCERTAINTY

	0 order	1st order	2nd order
TF before 70 s	4	$\frac{4}{s+1}$	$\frac{4}{(s+1)(s+5)}$
TF after 70 s	6	$\frac{6}{s+0.5}$	$\frac{6}{(s+0.5)(s+2.5)}$
$\bar{d}$	0.0154	0.0026	0.004
s	0.038	0.034	0.03
Mean conf. int.	$(-0.01, 0.04)$	$(-0.02, 0.025)$	$(-0.016, 0.023)$
St.d. conf. int.	$(0.026, 0.067)$	$(0.0235, 0.06)$	$(0.02, 0.05)$
Hypothesis test	H_0 is retained	H_0 is retained	H_0 is retained

Therefore, we cannot reject H_0. We retain H_0 and conclude that H_1 fails to be proved.

Since we are retaining the null hypothesis, we want to minimize the probability β of incorrectly retaining the null hypothesis. This means that we want our test's power, $1-\beta$, to be large, such as 0.95. What is the minimum required deviation of the population mean from 0, represented as μ_1, that would make our test to incorrectly retain the null hypothesis with 0.05 probability, i.e., $\beta = 0.05$? To calculate this, we first write the rejection region, R, using (46) as

$$R : \left|\frac{(\bar{d} - \mu_0)\sqrt{k}}{s}\right| \geq t_{\alpha/2} \implies R : |\bar{d}| \geq 0.0255. \qquad (47)$$

Defining $T = (((\bar{d} - \mu_1)\sqrt{k})/s)$, for $\beta = 0.05$, we need

$$P\left[\frac{(-0.0255 - \mu_1)\sqrt{k}}{s} < T < \frac{(0.0255 - \mu_1)\sqrt{k}}{s}\right] = \frac{\beta}{2} = 0.025. \qquad (48)$$

Using the t-table, it can be found that the minimum $|\mu_1|$ that satisfies (48) is 0.051. This means that our test can detect an 0.051 deviation from the mean value of the mean error between the adaptive human model and the participant data when the probability of the test to incorrectly conclude that the model and the data are compatible ($\mu_0 = 0$) is only 5%.

Analyses of the experimental results where a first-order plant dynamics is used with a sudden uncertainty injection is provided above. All of the results, including the ones for the other cases, where plants with different orders and sudden/gradual uncertainty injections, are summarized in Tables II and III. The data collected from the participants can be reached at http://www.syslab.bilkent.edu.tr/research.

VI. Summary

In this article, an adaptive human pilot model based on model reference adaptive control principles is proposed. This model mimics the pilot decision-making process by making sure that the overall closed-loop system follows the crossover model in the presence of plant uncertainties. The stability of the system is shown using the Lyapunov–Krasovskii stability criteria. Furthermore, experiments with human operators are conducted to validate the model. The detailed visual and statistical analyses of the experimental results show that the adaptive model creates similar system responses as the human operators.

Appendix

Proof of Theorem 5

Consider a Lyapunov–Krasovskii functional [39]

$$\begin{aligned} V(t) &= e^T Pe + \mathrm{tr}(\Phi^T(t)\Phi(t)) + \mathrm{tr}\big(\tilde{\theta}_1^T(t)\tilde{\theta}_1(t)\big) \\ &\quad + \int_{-\tau}^{0}\int_{t+\upsilon}^{t} \mathrm{tr}\big(\dot{\tilde{\theta}}_1^T(\xi)\dot{\tilde{\theta}}_1(\xi)\big)d\xi d\upsilon \\ &\quad + \int_{-\tau}^{0}\int_{t+\upsilon}^{t} \mathrm{tr}(\dot{\Phi}^T(\xi)\dot{\Phi}(\xi))d\xi d\upsilon \\ &\quad + \int_{-\tau}^{0} \mathrm{tr}\big(\tilde{\lambda}_1^T(t,\eta)\tilde{\lambda}_1(t,\eta)\big)d\eta \\ &\quad + \int_{-\tau}^{0}\int_{t+\upsilon}^{t}\int_{-\tau}^{0} \mathrm{tr}\big(\dot{\tilde{\lambda}}_1^T(\xi,\eta)\dot{\tilde{\lambda}}_1(\xi,\eta)\big)d\eta d\xi d\upsilon. \quad (49) \end{aligned}$$

The derivative of $V(t)$ can be calculated as

$$\begin{aligned} \dot{V}(t) &= \dot{e}^T(t)^T Pe(t) + e^T(t)P\dot{e}(t) + 2\mathrm{tr}\big(\dot{\tilde{\theta}}_1^T(t)\tilde{\theta}_1(t)\big) \\ &\quad + 2\mathrm{tr}(\dot{\Phi}^T(t)\Phi(t)) + \int_{-\tau}^{0} 2\mathrm{tr}\big(\dot{\tilde{\lambda}}_1^T(t,\eta)\tilde{\lambda}_1(t,\eta)\big)d\eta \\ &\quad + \tau\,\mathrm{tr}\big(\dot{\tilde{\theta}}_1^T(t)\dot{\tilde{\theta}}_1(t)\big) - \int_{-\tau}^{0} \mathrm{tr}\big(\dot{\tilde{\theta}}_1^T(t+\upsilon)\dot{\tilde{\theta}}_1(t+\upsilon)\big)d\upsilon \\ &\quad + \tau\,\mathrm{tr}(\dot{\Phi}^T(t)\dot{\Phi}(t)) - \int_{-\tau}^{0} \mathrm{tr}(\dot{\Phi}^T(t+\upsilon)\dot{\Phi}(t+\upsilon))d\upsilon \\ &\quad + \tau\int_{-\tau}^{0} \mathrm{tr}\big(\dot{\tilde{\lambda}}_1^T(t,\eta)\dot{\tilde{\lambda}}_1(t,\eta)\big)d\eta \\ &\quad - \int_{-\tau}^{0}\int_{-\tau}^{0} \mathrm{tr}\big(\dot{\tilde{\lambda}}_1^T(t+\upsilon,\eta)\dot{\tilde{\lambda}}_1(t+\upsilon,\eta)\big)d\eta d\upsilon. \quad (50) \end{aligned}$$

Substituting (24) into (50) and using the Lyapunov equation $A_m^T P + PA_m = -Q$, it is obtained that

$$\begin{aligned} \dot{V}(t) &= -e^T(t)Qe(t) + 2e^T(t)PB_m\tilde{\theta}_1(t-\tau)x_{hp}(t-\tau) \\ &\quad + 2e^T(t)PB_m\int_{-\tau}^{0}\tilde{\lambda}_1(t-\tau,\eta)u(t+\eta-\tau)d\eta \\ &\quad + 2e^T(t)PB_m\Phi(t-\tau)u(t-\tau) \\ &\quad + 2\mathrm{tr}\big(\dot{\tilde{\theta}}_1^T(t)\tilde{\theta}_1(t)\big) + 2\mathrm{tr}(\dot{\Phi}^T(t)\Phi(t)) \\ &\quad + \int_{-\tau}^{0} 2\mathrm{tr}\big(\dot{\tilde{\lambda}}_1^T(t,\eta)\tilde{\lambda}_1(t,\eta)\big)d\eta \\ &\quad + \tau\,\mathrm{tr}\big(\dot{\tilde{\theta}}_1^T(t)\dot{\tilde{\theta}}_1(t)\big) - \int_{-\tau}^{0} \mathrm{tr}\big(\dot{\tilde{\theta}}_1^T(t+\upsilon)\dot{\tilde{\theta}}_1(t+\upsilon)\big)d\upsilon \\ &\quad + \tau\,\mathrm{tr}(\dot{\Phi}^T(t)\dot{\Phi}(t)) - \int_{-\tau}^{0} \mathrm{tr}(\dot{\Phi}^T(t+\upsilon)\dot{\Phi}(t+\upsilon))d\upsilon \\ &\quad + \tau\int_{-\tau}^{0} \mathrm{tr}\big(\dot{\tilde{\lambda}}_1^T(t,\eta)\dot{\tilde{\lambda}}_1(t,\eta)\big)d\eta \\ &\quad - \int_{-\tau}^{0}\int_{-\tau}^{0} \mathrm{tr}\big(\dot{\tilde{\lambda}}_1^T(t+\upsilon,\eta)\dot{\tilde{\lambda}}_1(t+\upsilon,\eta)\big)d\eta d\upsilon. \end{aligned}$$

Using $g(t) - g(t-\tau) = \int_{-\tau}^{0} \dot{g}(t+\upsilon)d\upsilon$, (51) can be rewritten as

$$\begin{aligned} \dot{V}(t) &= -e^T(t)Qe(t) \\ &\quad + 2\mathrm{tr}\Big(x_{hp}(t-\tau)e^T(t)PB_m\tilde{\theta}_1(t) + \dot{\tilde{\theta}}_1^T(t)\tilde{\theta}_1(t)\Big) \\ &\quad + 2\mathrm{tr}\Big(u(t-\tau)e^T(t)PB_m\Phi(t) + \dot{\Phi}^T(t)\Phi(t)\Big) \\ &\quad + \int_{-\tau}^{0} 2\mathrm{tr}\Big(u(t+\eta-\tau)e^T(t)PB_m\tilde{\lambda}_1(t,\eta) \\ &\qquad + \dot{\tilde{\lambda}}_1^T(t,\eta)\tilde{\lambda}_1(t,\eta)\Big)d\eta \\ &\quad - 2e^T(t)PB_m\Big(\int_{-\tau}^{0}\dot{\tilde{\theta}}_1(t+\upsilon)d\upsilon\Big)x_{hp}(t-\tau) \\ &\quad - 2e^T(t)PB_m\Big(\int_{-\tau}^{0}\dot{\Phi}(t+\upsilon)d\upsilon\Big)u(t-\tau) \\ &\quad - 2e^T(t)PB_m\Big(\int_{-\tau}^{0}\Big(\int_{-\tau}^{0}\dot{\tilde{\lambda}}_1(t+\upsilon,\eta)d\upsilon\Big) \\ &\qquad \times u(t+\eta-\tau)d\eta\Big) \\ &\quad + \tau\,\mathrm{tr}\big(\dot{\tilde{\theta}}_1^T(t)\dot{\tilde{\theta}}_1(t)\big) - \int_{-\tau}^{0} \mathrm{tr}\big(\dot{\tilde{\theta}}_1^T(t+\upsilon)\dot{\tilde{\theta}}_1(t+\upsilon)\big)d\upsilon \\ &\quad + \tau\,\mathrm{tr}(\dot{\Phi}^T(t)\dot{\Phi}(t)) - \int_{-\tau}^{0} \mathrm{tr}(\dot{\Phi}^T(t+\upsilon)\dot{\Phi}(t+\upsilon))d\upsilon \\ &\quad + \tau\int_{-\tau}^{0} \mathrm{tr}\big(\dot{\tilde{\lambda}}_1^T(t,\eta)\dot{\tilde{\lambda}}_1(t,\eta)\big)d\eta \\ &\quad - \int_{-\tau}^{0}\int_{-\tau}^{0} \mathrm{tr}\big(\dot{\tilde{\lambda}}_1^T(t+\upsilon,\eta)\dot{\tilde{\lambda}}_1(t+\upsilon,\eta)\big)d\eta d\upsilon. \quad (51) \end{aligned}$$

By substituting (29)–(31) into (51), it is obtained that

$$\begin{aligned} &\dot{V}(t) \\ &= -e^T(t)Qe(t) \\ &\quad - 2\int_{-\tau}^{0} \mathrm{tr}(x_{hp}(t-\tau)e(t)^T PB_m\dot{\tilde{\theta}}_1(t+\upsilon))d\upsilon \\ &\quad - 2\int_{-\tau}^{0} \mathrm{tr}(u(t-\tau)e(t)^T PB_m\dot{\Phi}(t+\upsilon))d\upsilon \\ &\quad - 2\int_{-\tau}^{0}\int_{-\tau}^{0} \mathrm{tr}(u(t+\eta-\tau)e(t)^T PB_m\dot{\tilde{\lambda}}_1(t+\upsilon,\eta))d\upsilon d\eta \\ &\quad + \tau\,\mathrm{tr}\big(\dot{\tilde{\theta}}_1^T(t)\dot{\tilde{\theta}}_1(t)\big) - \int_{-\tau}^{0} \mathrm{tr}\big(\dot{\tilde{\theta}}_1^T(t+\upsilon)\dot{\tilde{\theta}}_1(t+\upsilon)\big)d\upsilon \\ &\quad + \tau\,\mathrm{tr}(\dot{\Phi}^T(t)\dot{\Phi}(t)) - \int_{-\tau}^{0} \mathrm{tr}(\dot{\Phi}^T(t+\upsilon)\dot{\Phi}(t+\upsilon))d\upsilon \\ &\quad + \tau\int_{-\tau}^{0} \mathrm{tr}\big(\dot{\tilde{\lambda}}_1^T(t,\eta)\dot{\tilde{\lambda}}_1(t,\eta)\big)d\eta \\ &\quad - \int_{-\tau}^{0}\int_{-\tau}^{0} \mathrm{tr}\big(\dot{\tilde{\lambda}}_1^T(t+\upsilon,\eta)\dot{\tilde{\lambda}}_1(t+\upsilon,\eta)\big)d\eta d\upsilon \\ &= -e^T(t)Qe(t) + \int_{-\tau}^{0} \mathrm{tr}\Big(2\dot{\tilde{\theta}}_1^T(t)\dot{\tilde{\theta}}_1(t+\upsilon) + \dot{\tilde{\theta}}_1^T(t)\dot{\tilde{\theta}}_1(t) \end{aligned}$$

$$- \dot{\tilde{\theta}}_1^T(t+\upsilon)\dot{\tilde{\theta}}_1(t+\upsilon)\Big)d\upsilon$$
$$+ \int_{-\tau}^{0} \mathrm{tr}\Big(2\dot{\Phi}^T(t)\dot{\Phi}(t+\upsilon) + \dot{\Phi}^T(t)\dot{\Phi}(t) - \dot{\Phi}^T(t+\upsilon)\dot{\Phi}(t+\upsilon)\Big)d\upsilon$$
$$+ \int_{-\tau}^{0}\int_{-\tau}^{0} \mathrm{tr}\Big(2\dot{\tilde{\lambda}}_1^T(t,\eta)\dot{\tilde{\lambda}}_1(t+\upsilon,\eta) + \dot{\tilde{\lambda}}_1^T(t,\eta)\dot{\tilde{\lambda}}_1(t,\eta) - \dot{\tilde{\lambda}}_1^T(t+\upsilon,\eta)\dot{\tilde{\lambda}}_1(t+\upsilon,\eta)\Big)d\eta d\upsilon. \quad (52)$$

Using the trace property $\mathrm{tr}(A+B) = \mathrm{tr}(A) + \mathrm{tr}(B)$ and the algebraic inequality $a^2 \geq 2ab - b^2$ for two scalars a and b, it can be shown that $\mathrm{tr}(2A^TB + A^TA - B^TB) \leq 2\mathrm{tr}(A^TA)$. Using these inequalities, (52) can be rewritten as

$$\dot{V}(t) \leq -e^T(t)Qe(t) + \int_{-\tau}^{0} 2\mathrm{tr}\big(\dot{\tilde{\theta}}_1^T(t)\dot{\tilde{\theta}}_1(t)\big)d\upsilon + \int_{-\tau}^{0} 2\mathrm{tr}(\dot{\Phi}^T(t)\dot{\Phi}(t))d\upsilon + \int_{-\tau}^{0}\int_{-\tau}^{0} 2\mathrm{tr}\big(\dot{\tilde{\lambda}}_1^T(t,\eta)\dot{\tilde{\lambda}}_1(t,\eta)\big)d\eta d\upsilon. \quad (53)$$

By substituting (29)–(31) into (53) and using the trace operator property $\mathrm{tr}(AB) = \mathrm{tr}(BA)$ for two square matrices A and B, (53) can be rewritten as

$$\begin{aligned}\dot{V}(t) \leq\ & -e^T(t)Qe(t) \\ & + 2\tau\,\mathrm{tr}\big(e(t)x_{hp}^T(t-\tau)x_{hp}(t-\tau)e(t)^TPB_mB_m^TP\big) \\ & + 2\tau\,\mathrm{tr}\big(e(t)u^T(t-\tau)u(t-\tau)e(t)^TPB_mB_m^TP\big) \\ & + 2\tau\int_{-\tau}^{0}\mathrm{tr}\big(e(t)u^T(t+\eta-\tau)u(t+\eta-\tau)e(t)^T \times PB_mB_m^TP\big)d\eta. \end{aligned} \quad (54)$$

Using $\mathrm{tr}(AB) \leq \mathrm{tr}(A)\mathrm{tr}(B)$ for two positive semidefinite matrices A and B and $\mathrm{tr}(X^TX) = \|X\|_F^2$ for a matrix X, an upper bound for (54) can be derived as

$$\begin{aligned}\dot{V}(t) \leq\ & -e^T(t)Qe(t) \\ & + 2\tau\,\mathrm{tr}(e(t)x_{hp}^T(t-\tau)x_{hp}(t-\tau)e(t)^T)\mathrm{tr}\big(PB_mB_m^TP\big) \\ & + 2\tau\,\mathrm{tr}\big(e(t)u^T(t-\tau)u(t-\tau)e(t)^T\big)\mathrm{tr}\big(PB_mB_m^TP\big) \\ & + 2\tau\int_{-\tau}^{0}\mathrm{tr}\big(e(t)u^T(t-\tau+\eta)u(t-\tau+\eta)e(t)^T\big) \times \mathrm{tr}\big(PB_mB_m^TP\big)d\eta \\ \leq\ & -\lambda_{\min}(Q)\|e(t)\|^2 \\ & + 2\tau\|x_{hp}(t-\tau)e(t)^T\|_F^2\big\|B_m^TP\big\|_F^2 \\ & + 2\tau\|u(t-\tau)e(t)^T\|_F^2\big\|B_m^TP\big\|_F^2 \\ & + 2\tau\int_{-\tau}^{0}\|u(t+\eta-\tau)e(t)^T\|_F^2\big\|B_m^TP\big\|_F^2d\eta \\ \leq\ & -\lambda_{\min}(Q)\|e(t)\|^2 \\ & + 2\tau\|x_{hp}(t-\tau)\|^2\|e(t)\|^2\big\|B_m^TP\big\|_F^2 \\ & + 2\tau\|u(t-\tau)\|^2\|e(t)\|^2\big\|B_m^TP\big\|_F^2 \\ & + 2\tau\int_{-\tau}^{0}\|u(t+\eta-\tau)\|^2\|e(t)\|^2\big\|B_m^TP\big\|_F^2d\eta \\ =\ & \big\|B_m^TP\big\|_F^2\|e(t)\|^2 \\ & \times\Big(-\frac{\lambda_{\min}(Q)}{\|B_m^TP\|_F^2} + 2\tau\Big(\|x_{hp}(t-\tau)\|^2 + \|u(t-\tau)\|^2 + \int_{-\tau}^{0}\|u(t+\eta-\tau)\|^2d\eta\Big)\Big). \end{aligned} \quad (55)$$

Defining $q \equiv ((\lambda_{\min}(Q))/(\|B_m^TP\|_F^2))$, the inequality

$$q - 2\tau\Big(\|x_{hp}(t-\tau)\|^2 + \|u(t-\tau)\|^2 + \int_{-\tau}^{0}\|u(t+\eta-\tau)\|^2d\eta\Big) > 0. \quad (56)$$

needs to be satisfied for the nonpositiveness of $\dot{V}$. Assuming that x_{hp} and u are bounded in the interval $[t_0-2\tau, t_0)$, the rest of the proof is divided into the following four steps.

Step 1: In this step, the negative semidefiniteness of the Lyapunov–Krasovskii functional's (49) time derivative in the interval $[t_0-\tau, t_0)$ is shown, which leads to the boundedness of the signals in this interval. In addition, an upper bound for u in the interval $[t_0-2\tau, t_0)$ is given.

Suppose that

$$\sup_{\xi\in[t_0-\tau,t_0)}\|x_{hp}(\xi)\|^2 \leq \gamma_1 \qquad \sup_{\xi\in[t_0-2\tau,t_0)}\|u(\xi)\|^2 \leq \gamma_2 \quad (57)$$

for some positive $\gamma_1|$ and γ_2, and τ_1 is given such that

$$2\tau_1(\gamma_1 + \gamma_2 + \tau_1\gamma_2) < q. \quad (58)$$

Then, the following inequality is satisfied:

$$q - 2\tau\Big(\|x_{hp}(\xi-\tau)\|^2 + \|u(\xi-\tau)\|^2 + \int_{-\tau}^{0}\|u(\xi+\eta-\tau)\|^2d\eta\Big) > 0 \quad \forall\xi\in[t_0,t_0+\tau)\ \ \forall\tau\in[0,\tau_1]. \quad (59)$$

It follows that $V(t)$, defined in (49), is nonincreasing for $t \in [t_0, t_0+\tau)$. Thus, we have

$$\lambda_{\min}(P)\|e(\xi)\|^2 \leq e(\xi)^TPe(\xi) \leq V(t_0) \quad (60)$$

which leads to

$$\|x_{hp}(\xi)\| - \|x_m(\xi)\| \leq \|e(\xi)\| \leq \sqrt{\frac{V(t_0)}{\lambda_{\min}(P)}}. \quad (61)$$

Then, we have

$$\|x_{hp}(\xi)\| \leq \sqrt{\frac{V(t_0)}{\lambda_{\min}(P)}} + \|x_m(\xi)\| \quad (62)$$

for $\forall\xi \in [t_0, t_0+\tau)$. We also have the inequality

$$\|\Phi(\xi)\|^2 \leq V(t_0) \implies \big\|K_r^{*-1} - K_r^{-1}(\xi)\big\|^2 \leq V(t_0) \implies \big\|K_r^{-1}(\xi)\big\| \leq \sqrt{V(t_0)} + \big\|K_r^{*-1}\big\| \quad (63)$$

for $\forall\xi \in [t_0, t_0+\tau)$. It is noted that the boundedness of $\Phi = K_r^{*-1} - K_r^{-1}$ does not guarantee the boundedness of $\tilde{K}_r$. In order to guarantee the boundedness of $\tilde{K}_r$ independent

of the boundedness of Φ, the projection algorithm [40] is employed as

$$\dot{K}_r = \text{Proj}\big(K_r, -K_r B_m^T P e(t) u^T(t-\tau) K_r\big) \tag{64}$$

with an upper bound $K_{\max}$, that is, $\|K_r\| \leq K_{\max}$. Thus, a lower bound for $\|K_r^{-1}(\xi)\|$ can be calculated using the following algebraic manipulations:

$$\begin{aligned} &K_r(\xi)K_r^{-1}(\xi) \\ &\quad = I \Rightarrow \big\|K_r(\xi)K_r^{-1}(\xi)\big\| = 1 \\ &\qquad \Rightarrow 1 \leq \|K_r(\xi)\|\big\|K_r^{-1}(\xi)\big\| \leq K_{\max}\big\|K_r^{-1}(\xi)\big\| \\ &\qquad \Rightarrow \frac{1}{K_{\max}} \leq \big\|K_r^{-1}(\xi)\big\|. \end{aligned} \tag{65}$$

Defining $k_1 = \sqrt{V(t_0)} + \|K_r^{*-1}\|$ and using (63), it is obtained that

$$\frac{1}{K_{\max}} \leq \big\|K_r^{-1}(\xi)\big\| \leq k_1, \quad \xi \in [t_0, t_0+\tau). \tag{66}$$

Therefore, K_r is always bounded and $K_r^{-1}(\xi)$ is bounded for $\forall \xi \in [t_0, t_0+\tau)$.

Furthermore, using the definitions of $\theta_x, \theta_1, \lambda$, and λ_1 given in Theorem 5, and the nonincreasing Lyapunov functional (49), it can be concluded that

$$\|\tilde{\theta}_1(\xi)\|_F^2 \leq V(t_0) \implies \big\|\tilde{K}_r^{-1}(\xi)\tilde{\theta}_x(\xi)\big\|_F^2 \leq V(t_0) \tag{67}$$

$$\begin{aligned} \int_{-\tau}^{0} \|\tilde{\lambda}_1(\xi,\eta)\|_F^2 d\eta \quad &\leq \quad V(t_0) \\ &\implies \int_{-\tau}^{0} \big\|K_r^{-1}(\xi)\tilde{\lambda}(\xi,\eta)\big\|_F^2 d\eta \leq V(t_0) \end{aligned} \tag{68}$$

for $\forall \xi \in [t_0, t_0+\tau)$. Using (67) and (68), it can be obtained that

$$\begin{aligned} \|\tilde{\theta}_x(\xi)\|_F^2 &\leq K_{\max}^2 V(t_0) \\ \int_{-\tau}^{0} \|\tilde{\lambda}(\xi,\eta)\|_F^2 d\eta &\leq K_{\max}^2 V(t_0) \end{aligned} \tag{69}$$

for $\forall \xi \in [t_0, t_0+\tau)$.

To simplify the notation, we define

$$\begin{aligned} I_0 \equiv \max\Bigg(&\sqrt{\frac{V(t_0)}{\lambda_{\min}(P)}} + \sup_{[t_0, t_0+\tau)} \|x_m(\xi)\|, \\ &K_{\max}\sqrt{V(t_0)}, K_{\max}^2 V(t_0)\Bigg) \end{aligned} \tag{70}$$

where $R_{\max}$ is the upper bound of the reference input $r(t)$.

An upper bound on the control signal $u(t)$ for $t \in [t_0, t_0+\tau)$ can be derived by using Lemma 4 and (15). In particular, setting $t_i' = t_0$, $t_j' = t_0 + \tau$, and $c_0^2 = V(t_0)$, we obtain that

$$|u(\xi)| \leq 2\Bigg(\bar{f} + \Bigg(\int_{-\tau}^{0} u^2(t_0+\eta)d\eta\Bigg)^{1/2} I_0\Bigg) e^{I_0 \tau} \tag{71}$$

for $\forall \xi \in [t_0, t_0+\tau)$, where $\bar{f}$, which is the upper bound of $\theta_x(t)x_{hp}(t) + K_r(t)r(t)$, depends only on I_0. Defining $g(\gamma_2, I_0, \tau) \equiv 2(\bar{f} + \gamma_2 I_0 \sqrt{\tau}) e^{I_0 \tau}$, (71) can be rewritten as

$$|u(\xi)| \leq g(\gamma_2, I_0, \tau) \quad \forall \xi \in [t_0, t_0+\tau). \tag{72}$$

The rest of the proof is similar to the one given in [39]. In the following, a summary of the next steps are given.

Step 2: A delay range $[0, \tau_2]$ is found, which satisfies the condition (56) over the interval $[t_0, t_0+2\tau)$ as

$$2\tau_2\big(I_0^2 + (\max(\gamma_2, g(\gamma_2, I_0, \tau_2)))^2(1+\tau_2)\big) < q \tag{73}$$

which leads to $\|x_{hp}(\xi)\| < I_0$, $\forall \xi \in [t_0, t_0+2\tau)$, $\forall \tau \in [0, \bar{\tau}_2]$, $\bar{\tau}_2 = \min\{\tau_1, \tau_2\}$.

Step 3: It is shown in this step that the bound on u over the interval $[t_0, t_0+\tau)$ depends only on A_{hp}, B_{hp}, T, and τ, where T is a value between t_0 and τ. Denoting this upper bound as $U(I_0)$, we have $|u(t)| \leq U(I_0)$, $t \in [t_0, t_0+\tau)$.

Step 4: Using the calculated upper bound for u in the previous step, a delay range $[0, \tau_2]$ is found, which satisfies the condition

$$2\tau_3\big(I_0^2 + (\max(U(I_0), g(U(I_0), I_0, \tau_3)))^2(1+\tau_3)\big) < q. \tag{74}$$

For $\tau^* = \min(\bar{\tau}_2, \tau_3)$, $\|x_{hp}(\xi)\| \leq I_0$ and $|u(\xi)| \leq U(I_0)$ for all $\xi \in [t_0, t_0+\tau]$, $\forall \tau \in [0, \tau^*]$.

The above four steps show that $x_{hp}(\xi)$ and $u(\xi)$ are bounded for $\forall \xi \in [t_0, t_0+k\tau]$, for $k=1$ and $\tau \in (0, \tau^*]$. By assuming that x_{hp} and u are bounded for a given k, the rest of the proof consists of showing that the boundedness of these variables hold for $k+1$. Using this assumption and repeating steps 1–4, which leads to satisfying (74), we conclude that the Lyapunov function is nonincreasing and $\|x_{hp}(\xi)\| \leq I_0$, and $|u(\xi)| \leq g(U(I_0), I_0, \tau)$ for $\xi \in [t_0, t_0+(k+1)\tau]$, $\tau \leq \tau^* \leq \tau_3$. This completes the boundedness proof using induction. Then, using Barbalat's Lemma, it can be shown that the error between the human-in-the-loop system output x_{hp} and the reference model output x_m converges to zero.

REFERENCES

[1] W. D. Nothwang, M. J. McCourt, R. M. Robinson, S. A. Burden, and J. W. Curtis, "The human should be part of the control loop?" in *Proc. Resilience Week (RWS)*, Aug. 2016, pp. 214–220.

[2] M. Korber, W. Schneider, and M. Zimmermann, "Vigilance, boredom proneness and detection time of a malfunction in partially automated driving," in *Proc. Int. Conf. Collaboration Technol. Syst. (CTS)*, Jun. 2015, pp. 70–76.

[3] Y. Yildiz and I. V. Kolmanovsky, "A control allocation technique to recover from pilot-induced oscillations (capio) due to actuator rate limiting," in *Proc. Amer. Control Conf.*, Jun. 2010, pp. 516–523.

[4] Y. Yildiz and I. Kolmanovsky, "Stability properties and cross-coupling performance of the control allocation scheme CAPIO," *J. Guid., Control, Dyn.*, vol. 34, no. 4, pp. 1190–1196, Jul. 2011.

[5] D. M. Acosta *et al.*, "Piloted evaluation of a control allocation technique to recover from pilot-induced oscillations," *J. Aircr.*, vol. 52, no. 1, pp. 130–140, Jan. 2015.

[6] S. S. Tohidi, Y. Yildiz, and I. Kolmanovsky, "Pilot induced oscillation mitigation for unmanned aircraft systems: An adaptive control allocation approach," in *Proc. IEEE Conf. Control Technol. Appl. (CCTA)*, Aug. 2018, pp. 343–348.

[7] W. Li, D. Sadigh, S. S. Sastry, and S. A. Seshia, "Synthesis for human-in-the-loop control systems," in *Proc. Int. Conf. Tools Algorithms Construct. Anal. Syst.*, Cham, Switzerland: Springer, 2014, pp. 470–484.

[8] T. Hulin, A. Albu-Schaffer, and G. Hirzinger, "Passivity and stability boundaries for haptic systems with time delay," *IEEE Trans. Control Syst. Technol.*, vol. 22, no. 4, pp. 1297–1309, Jul. 2014.

[9] T. Yucelen, Y. Yildiz, R. Sipahi, E. Yousefi, and N. Nguyen, "Stability limit of human-in-the-loop model reference adaptive control architectures," *Int. J. Control*, vol. 91, no. 10, pp. 2314–2331, Oct. 2018.

[10] E. Eraslan, Y. Yildiz, and A. M. Annaswamy, "Shared control between pilots and autopilots: An illustration of a cyberphysical human system," *IEEE Control Syst.*, vol. 40, no. 6, pp. 77–97, Dec. 2020.

[11] J. Zhao and T. Iwasaki, "CPG control for harmonic motion of assistive robot with human motor control identification," *IEEE Trans. Control Syst. Technol.*, vol. 28, no. 4, pp. 1323–1336, Jul. 2020.

[12] D. T. McRuer and E. S. Krendel, "Dynamic response of human operators," Tech. Rep. WADC-TR-56-524, 1957.

[13] D. T. McRuer and E. S. Krendel, "Mathematical models of human pilot behavior," Tech. Rep. AGARD-AG-188, 1974.

[14] T. P. Neal and R. E. Smith, "A flying qualities criterion for the design of fighter flight-control systems," *J. Aircr.*, vol. 8, no. 10, pp. 803–809, Oct. 1971.

[15] D. Mcruer and D. Graham, "Pilot-vehicle control system analysis," in *Proc. Guid. Control Conf.*, Aug. 1963, p. 310.

[16] G. Beerens, H. Damveld, M. Mulder, and M. Van Paassen, "An investigation into crossover regression and pilot parameter adjustment," in *Proc. AIAA Model. Simul. Technol. Conf. Exhib.*, Aug. 2008, p. 7112.

[17] M. Martinez-Garcia, T. Gordon, and L. Shu, "Extended crossover model for human-control of fractional order plants," *IEEE Access*, vol. 5, pp. 27622–27635, 2017.

[18] R. B. Warrier and S. Devasia, "Inferring intent for novice human-in-the-loop iterative learning control," *IEEE Trans. Control Syst. Technol.*, vol. 25, no. 5, pp. 1698–1710, Sep. 2017.

[19] J. J. Gil, A. Rubio, and J. Savall, "Decreasing the apparent inertia of an impedance haptic device by using force feedforward," *IEEE Trans. Control Syst. Technol.*, vol. 17, no. 4, pp. 833–838, Jul. 2009.

[20] R. D. Wierenga, "An evaluation of a pilot model based on Kalman filtering and optimal control," *IEEE Trans. Man-Mach. Syst.*, vol. MMS-10, no. 4, pp. 108–117, Dec. 1969.

[21] D. L. Kleinman, S. Baron, and W. H. Levison, "An optimal control model of human response—Part I: Theory and validation," *Automatica*, vol. 6, no. 3, pp. 357–369, May 1970.

[22] X. Na and D. J. Cole, "Modelling and identification of a driver controlling a vehicle equipped with active steering where the driver and vehicle have different target paths," in *Proc. 11th Int. Symp. Adv. Vehicle Control (AVEC)*, 2012.

[23] M. M. Lone and A. K. Cooke, "Pilot-model-in-the-loop simulation environment to study large aircraft dynamics," *Proc. Inst. Mech. Eng., G, J. Aerosp. Eng.*, vol. 227, no. 3, pp. 555–568, Mar. 2013.

[24] W.-L. Hu, C. Rivetta, E. MacDonald, and D. P. Chassin, "Optimal operator training reference models for human-in-the-loop systems," in *Proc. Annu. Hawaii Int. Conf. Syst. Sci.*, 2019, pp. 1–8.

[25] R. A. Hess, "Modeling pilot control behavior with sudden changes in vehicle dynamics," *J. Aircr.*, vol. 46, no. 5, pp. 1584–1592, Sep. 2009.

[26] R. A. Hess, "Modeling human pilot adaptation to flight control anomalies and changing task demands," *J. Guid., Control, Dyn.*, vol. 39, no. 3, pp. 655–666, Mar. 2016.

[27] S. Xu, W. Tan, and X. Qu, "Modeling human pilot behavior for aircraft with a smart inceptor," *IEEE Trans. Human-Mach. Syst.*, vol. 49, no. 6, pp. 661–671, Dec. 2019.

[28] M. Lone and A. Cooke, "Review of pilot models used in aircraft flight dynamics," *Aerosp. Sci. Technol.*, vol. 34, pp. 55–74, Apr. 2014.

[29] S. Xu, W. Tan, A. V. Efremov, L. Sun, and X. Qu, "Review of control models for human pilot behavior," *Annu. Rev. Control*, vol. 44, pp. 274–291, Jan. 2017.

[30] P. Zaal and B. Sweet, "Estimation of time-varying pilot model parameters," in *Proc. AIAA Modeling Simulation Technol. Conf.*, Aug. 2011, p. 6474.

[31] R. F. M. Duarte, D. M. Pool, M. M. van Paassen, and M. Mulder, "Experimental scheduling functions for global LPV human controller modeling," *IFAC-PapersOnLine*, vol. 50, no. 1, pp. 15853–15858, Jul. 2017.

[32] X. Zhang, T. M. Seigler, and J. B. Hoagg, "Modeling the control strategies that humans use to control nonminimum-phase systems," in *Proc. Amer. Control Conf. (ACC)*, Jul. 2015, pp. 471–476.

[33] K. van der El, D. M. Pool, H. J. Damveld, M. R. M. van Paassen, and M. Mulder, "An empirical human controller model for preview tracking tasks," *IEEE Trans. Cybern.*, vol. 46, no. 11, pp. 2609–2621, Nov. 2016.

[34] S. S. Tohidi and Y. Yildiz, "Adaptive human pilot model for uncertain systems," in *Proc. 18th Eur. Control Conf. (ECC)*, Jun. 2019, pp. 2938–2943.

[35] D. T. McRuer and H. R. Jex, "A review of quasi-linear pilot models," *IEEE Trans. Hum. Factors Electron.*, vol. HFE-8, no. 3, pp. 231–249, Sep. 1967.

[36] R. E. Magdaleno, *Experimental Validation and Analytical Elaboration for Models of the Pilot's Neuromuscular Sub-System in Tracking Tasks*, vol. 1757, Washington, DC, USA: NASA, 1971.

[37] M. M. van Paasen, J. C. van der Vaart, and J. A. Mulder, "Model of the neuromuscular dynamics of the human Pilot's arm," *J. Aircr.*, vol. 41, no. 6, pp. 1482–1490, Nov. 2004.

[38] K. S. Narendra and A. M. Annaswamy, *Stable Adaptive Systems*. Chelmsford, MA, USA: Courier Corporation, 2012.

[39] Y. Yildiz, A. Annaswamy, I. V. Kolmanovsky, and D. Yanakiev, "Adaptive posicast controller for time-delay systems with relative degree $n^* \leq 2$," *Automatica*, vol. 46, no. 2, pp. 279–289, 2010.

[40] E. Lavretsky and K. A. Wise, *Robust Adaptive Control*. Springer, 2013, pp. 317–353.

[41] S. S. Tohidi and Y. Yildiz, "Handling actuator magnitude and rate saturation in uncertain over-actuated systems: A modified projection algorithm approach," *Int. J. Control*, vol. 95, pp. 1–14, Sep. 2020.

[42] S. Barendswaard, D. M. Pool, M. M. Van Paassen, and M. Mulder, "Dual-axis manual control: Performance degradation, axis asymmetry, crossfeed, and intermittency," *IEEE Trans. Human-Mach. Syst.*, vol. 49, no. 2, pp. 113–125, Apr. 2019.

[43] Y. Yildiz, A. M. Annaswamy, D. Yanakiev, and I. Kolmanovsky, "Spark-ignition-engine idle speed control: An adaptive control approach," *IEEE Trans. Control Syst. Technol.*, vol. 19, no. 5, pp. 990–1002, Sep. 2011.

[44] A. Alan, Y. Yildiz, and U. Poyraz, "High-performance adaptive pressure control in the presence of time delays: Pressure control for use in variable-thrust rocket development," *IEEE Control Syst.*, vol. 38, no. 5, pp. 26–52, Oct. 2018.

[45] N. Olgac and R. Sipahi, "An exact method for the stability analysis of time-delayed linear time-invariant (LTI) systems," *IEEE Trans. Autom. Control*, vol. 47, no. 5, pp. 793–797, May 2002.

[46] R. A. Johnson and G. K. Bhattacharyya, *Statistics: Principles and Methods*. Hoboken, NJ, USA: Wiley, 2019.

Seyed Shahabaldin Tohidi received the B.S. degree in electrical engineering from the Shiraz University of Technology, Shiraz, Iran, in 2010, the M.S. degree in electrical engineering from the K. N. Toosi University of Technology, Tehran, Iran, in 2014, and the Ph.D. degree in from the Department of Mechanical Engineering, Bilkent University, Ankara, Turkey, in 2021.

He is currently a Post-Doctoral Researcher with the Applied Mathematics and Computer Science Department, Technical University of Denmark, Kongens Lyngby, Denmark. His research interests include adaptive control, stochastic control, advanced modeling, optimization, cyber-physical human systems, and their application in energy systems and smart cities.

Yildiray Yildiz (Senior Member, IEEE) received the B.S. degree in mechanical engineering from Middle East Technical University (METU), Ankara, Turkey, in 2002, the M.S. degree in mechatronics from Sabancı University, Istanbul, Turkey, in 2004, and the Ph.D. degree in mechanical engineering from the Massachusetts Institute of Technology, Cambridge, MA, USA, in 2009.

He held post-doctoral and associate scientist positions with the NASA Ames Research Center, Mountain View, CA, USA, employed by the University of California at Santa Cruz, Santa Cruz, CA, USA, through its university-affiliated research center, from 2009 to 2014. He is currently an Assistant Professor with Bilkent University, Ankara. His research interests include controls and machine learning.

Dr. Yildiz was a member of the IEEE CSS Board of Governors in 2020. He was a recipient of the NASA Honor Award, the Young Scientist Award from the Science Academy of Turkey, the Young Scientist Award from the Turkish Academy of Sciences, the Research Incentive Award from the Parlar Foundation, and the Best Student Conference Paper Award from the American Society of Mechanical Engineers (ASME). He is serving as an Associate Editor for IEEE Control Systems Society, IEEE TRANSACTIONS ON CONTROL SYSTEMS TECHNOLOGY, and *European Journal of Control*.